Chemical Engineering Science 143 (2016) 305–313

Contents lists available at ScienceDirect

Chemical Engineering Science

journal homepage: www.elsevier.com/locate/ces

Mass transfer limitations in a monolithic reactor for the catalytic oxidation of ethanol

M.L. Rodríguez *, L.E. Cadús

INTEQUI (UNLS/CONICET), Chacabuco y Pedernera, San Luis, Argentina

HIGHLIGHTS

- Catalytic oxidation of ethanol in a monolithic ceramic reactor is modelled.
- Significant diffusional resistances at low operating temperatures are found.
- Process rate is reduced by internal mass transfer resistances at high VOC conversions.
- Poor interfacial areas lead to significant external mass transfer resistances.

GRAPHICAL ABSTRACT

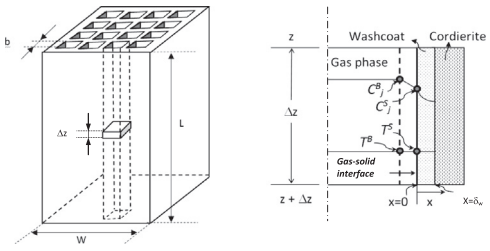

ARTICLE INFO

Article history:
Received 11 July 2015
Received in revised form
13 October 2015
Accepted 19 December 2015
Available online 29 December 2015

Keywords:
Catalytic oxidation
Monolithic reactor
Heterogeneous model
Mass transfer
Ethanol

ABSTRACT

A theoretical study of a monolithic reactor for the catalytic oxidation of Volatile Organic Compounds (VOC) over manganese–copper mixed oxide catalysts is presented. An isothermal one-dimensional heterogeneous model is selected to account for the external (gas–solid) and internal (washcoat) mass transport limitations.

The results reveal that under certain operating conditions, e.g. thick washcoats and high conversions of VOCs (high temperatures), the overall process rate is reduced by internal diffusion inside the catalyst. At high temperatures and/or monoliths with poor interfacial areas, the overall process rate is limited by external mass transfer resistance to the catalyst. Proper quantification of both internal and external mass transfer resistances by means of a heterogeneous model can result in avoiding situations of incomplete VOC abatement under conditions of high VOC dilution.

1. Introduction

The pollutant emission control such as Volatile Organic Compounds is one of the priorities of environmental catalysis (Everaert and Baeyens, 2004; Heck et al., 2009; Khan and Ghoshal, 2000). Increasingly tighter and more precise global standards exist towards controlling the emissions of these dangerous pollutants (Air Quality Guidelines – WHO, 2005; The Clean Air Act – EPA, 2004). The European Commission (http://ec.europa.eu/environment/air/legis.htm) sets an emission limit value of 20 mg/Nm^3 in the stream discharged into the atmosphere.

VOCs emissions affect the climate change, plants growth and decay and human beings and animal's health. Despite their undeniable danger, their use is widely spread because of their degreasing/solvent properties. VOCs are emitted by both, industries that synthesise them and industries that generate them as by-products or use them in their processes.

Technology to reduce VOC emissions is selected according to the temperature and composition of the VOC contained by the stream, the volumetric flow rate of the emission, the available site for the installation and operating costs. VOC concentrations in the air streams are often in the 50–2000 ppm range and flow rates in the 1000–10,000 scfm (1700–17,000 m^3/h) range are common (Wang et al., 2001). Catalytic oxidation as a removal method is a particularly suitable technology for treating emissions at low VOC

* Corresponding author. Tel.: +54 2657 531000x7039; fax: +54 2657 531000.
E-mail address: mlrodri@unsl.edu.ar (M.L. Rodríguez).

http://dx.doi.org/10.1016/j.ces.2015.12.010
0009-2509/

concentrations since the total oxidation of diluted fuels occurs at relatively low temperatures leading to low emissions of NO_x and unburned fuels (Everaert and Baeyens, 2004; Mitsui et al., 2009).

Thus, not only a suitable catalyst is important but also an appropriate reactor configuration to process large volumes of air+VOC emissions with low pressure drops.

Due to the diverse nature of VOCs, as well as the volume and composition of the industrial emissions, the monolithic reactors become particularly attractive to perform the catalytic removal. The major advantages of this design are low pressure drop under high fluid throughputs leading to an energy-efficient operation, short diffusion path in the catalyst and high external surface area, among others (Avila et al., 2005; Chen et al., 2008; Heck et al., 2001; Tomasic and Jovic, 2006).

Considerable effort has been directed towards obtaining suitable catalysts for catalytic oxidation (Choudhary et al., 2002; Ertl et al., 2008). The Mn–Cu mixed oxide catalyst formulated by Morales et al. (2008) demonstrated to be highly active at moderate temperatures for the catalytic oxidation of a wide number of VOCs. This catalyst has been successfully deposited by impregnation on ceramic monoliths (Agüero et al., 2013), setting the most appropriate features to perform the VOC catalytic combustion process in a single device.

Ethyl acetate and ethanol are the predominant VOC in the printing industry. These processes generally present temporal VOC emission patterns. When VOC concentration decreases to a few hundred part per millions (ppm), the heat generation caused by the evolution of oxidation reactions is very low and may lead to a non-effective pollutant removal.

Detailed modelling and simulation of monolith reactors contribute to understand the complexity of interactions between various physical and chemical processes that occur within the channels and inside the channel coating (Chen et al., 2008) playing a significant role in the design of these systems. The correct interpretation of the mass transfer phenomena occurring in the process is essential to define operating and design conditions to achieve a complete removal of VOCs (Hayes and Kolaczkowski, 1997).

In previous researches, for washcoat thickness less than 50 μm, diffusion resistances were assumed to be negligible. However, more recent studies have shown that this may not be so (Gonzo, 2008; Hayes et al., 2004). Hayes and Kolaczkowski (1994) found that when temperature is high (> 700 °C), internal diffusion limitations could be significant even with a very thin washcoat thickness. Metkar et al. (2011) observed washcoat diffusion limitations for the standard SCR reaction (NH_3+NO+O_2) on a Cu-zeolite catalyst at low temperatures starting at 250 °C. It was also found that the contribution of external mass transfer was significant under certain conditions.

The Mn–Cu mixed oxide powder catalyst (particle size: 500–841 μm) presents a strong influence of intraparticle mass transfer at temperatures between 217 and 229 °C. Thus, the effectiveness factor for ethanol combustion varies between 0.013 and 0.220 along the reactor (Campesi et al., 2011).

In the present article, a theoretical study of a monolithic reactor for the catalytic oxidation of ethanol over Mn–Cu mixed oxide catalysts is presented. The effect of the interphase and intraphase mass transport limitations at high VOC dilution is analysed by means of a 1D heterogeneous model. The influence of the main operating variables on the reactor performance is also studied.

2. Mathematical model

2.1. Model equations

Fig. 1 shows the schematic representation of the design under study. A stream of ethanol diluted in air enters the ceramic monolithic reactor. The channels of a ceramic monolith of square section are covered by the Mn–Cu mixed oxide catalyst with an atomic ratio of 9:1 (Agüero et al., 2013).

The reaction scheme considered in this work is shown in Table 1. A system of two reactions in series is considered, which includes the partial oxidation of ethanol to acetaldehyde (Reaction 1) and the total oxidation of acetaldehyde (Reaction 2). The kinetic expressions and the kinetic parameters given by Campesi et al. (2011) for the Mn–Cu catalyst are adopted and presented in Tables 1 and 2, respectively.

A one-dimensional heterogeneous model to represent the steady-state operation of the monolithic reactor is proposed. It is assumed that the gas-phase temperature, composition and velocity are uniform across the monolith cross-section. The following additional hypotheses are adopted:

- Isobaric conditions: a total developed laminar flow is assumed through the channels, leading to a low pressure drop.
- Isothermal conditions: the high dilution of the VOC in the inlet stream supports this hypothesis. Estimations of the temperature drop over the film were calculated according to the guidelines of Froment and Bischoff (1990). The overall temperature gradients in the gas diffusion layer are lower than 1.5 °C for all the explored operating conditions.
- Axial dispersion of mass is neglected: longitudinal mass Peclet number (Pe) $\gg 2$ demonstrates that the flow behaviour of the gas phase is plug flow type (Hessel et al., 2005).
- Unidirectional flow inside the monolith channel is assumed.
- The catalytic material accumulation in the corners of the square channels is negligible.
- A single channel is considered as representative of the entire reactor: size and shape of the channels, catalyst activity and gas flow distribution between the channels are assumed uniform (Hayes and Kolaczkowski, 1997).
- Ideal gas is assumed.

Based on these assumptions, the reactor is represented by the following equations:

Gas phase

Mass balances

$$\frac{dC_{Et}}{dz} = -\frac{1}{u}\frac{V_w}{V_g}\eta_1 r_1^s \tag{3}$$

$$\frac{dC_{Ac}}{dz} = \frac{1}{u}\frac{V_w}{V_g}(\eta_1 r_1^s - \eta_2 r_2^s) \tag{4}$$

where

$$\eta_i = \frac{\int_0^{V_w} r_i(C_{s,j})\,dV_w}{V_w r_i\left(C_{s,j}^s\right)} = \frac{r_i^{eff}}{r_i^s} \quad \text{with } i = 1,2 \tag{5}$$

Initial conditions:

$$\text{At } z = 0 : C_j = C_{0j} \tag{6}$$

Solid phase (washcoat)

Mass balances

$$D_{e,Et}\frac{d^2 C_{s,Et}}{dx^2} = -\rho_w r_1(C_{s,j}) \tag{7}$$

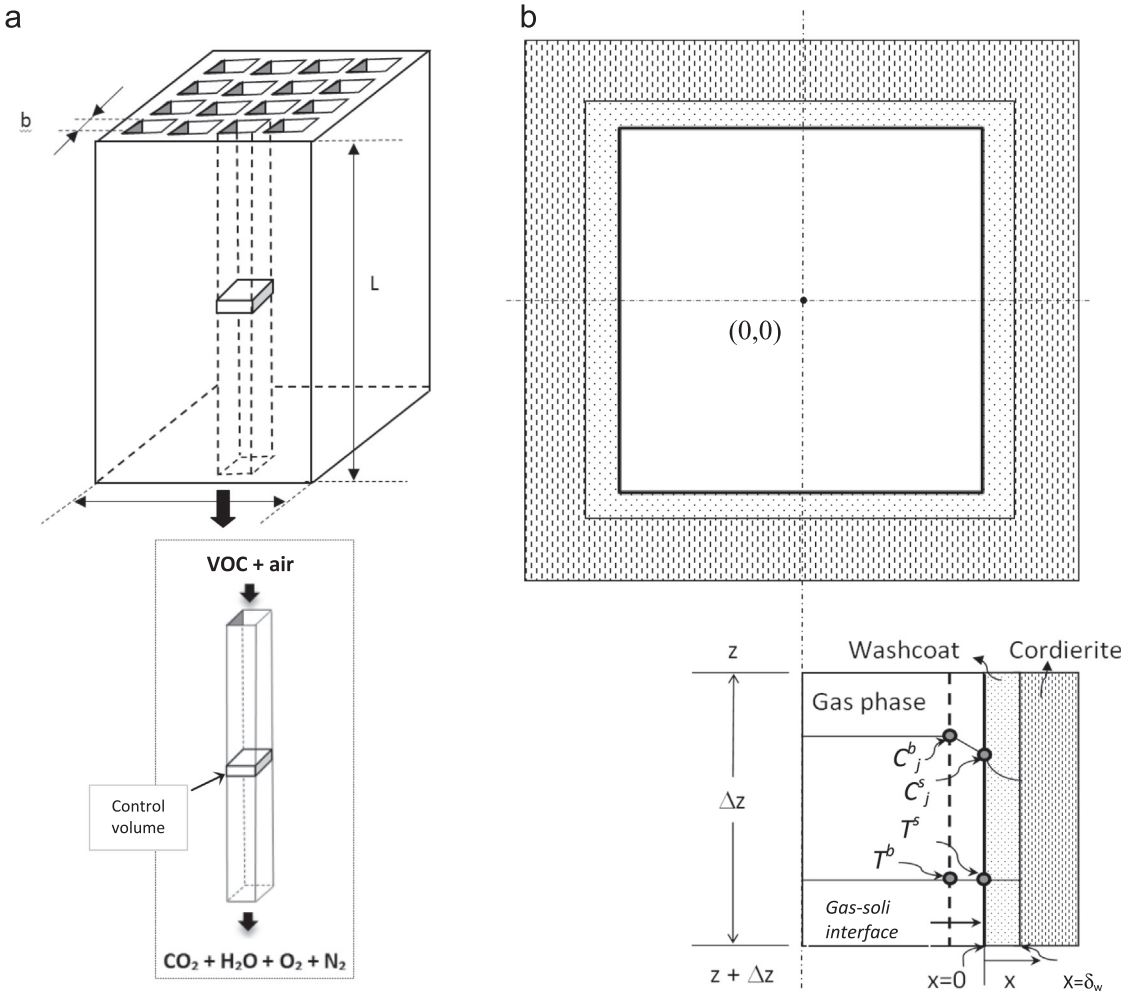

Fig. 1. (a) Monolith reactor and representative channel schematic representation. (b) Cross-section of a channel with uniform washcoat thickness and diffusional resistances scheme.

Table 1
Reaction system and kinetic expressions (Campesi et al., 2011).

Reaction system	Kinetic expressions
$C_2H_6O+(1/2)O_2 \rightarrow C_2H_4O+H_2O$	$r_1=\frac{k_{ref,1}\exp[-(E_1/R)(1/T-1/T_{ref})]C_{Et}}{1+Kc_{ET}C_{Et}+Kc_{Ac}C_{Ac}}$ (1)
$C_2H_4O+(5/2)O_2 \rightarrow 2CO_2+2H_2O$	$r_2=\frac{k_{ref,2}\exp[-(E_2/R)(1/T-1/T_{ref})]Kc_{Ac}C_{Ac}}{1+Kc_{ET}C_{Et}+Kc_{Ac}C_{Ac}}$ (2)

Table 2
Kinetic parameters (Campesi et al., 2011).

Parameter	Optimal value and confidence interval
$k_{ref,1}$	$(1.81 \pm 0.3) \times 10^3$ s^{-1}
$k_{ref,2}$	$(1.81 \pm 0.26) \times 10^{-1}$ mol s^{-1} m^{-3}
E_1	$(1.10 \pm 0.04) \times 10^5$ J mol^{-1}
E_2	$(1.69 \pm 0.09) \times 10^5$ J mol^{-1}
Kc_{Et}	~ 0
Kc_{Ac}	$(6.75 \pm 1.26) \times 10^2$ m^3 mol^{-1}

$$D_{e,Ac}\frac{d^2C_{s,Ac}}{dx^2}=\rho_w(r_1(C_{s,j})-r_2(C_{s,j})) \quad (8)$$

Boundary conditions:
At $x=0$:

$$k_{g,j}\left(C_j-C^s_{s,j}\right)=-D_{e,j}\left(\frac{dC_{s,j}}{dx}\right)|_{x=0} \quad (9)$$

At $x=\delta_w$:

$$\frac{dC_{s,j}}{dx}=0 \quad \text{with } j=Et,Ac \quad (10)$$

A pore radius of 120 Å, a washcoat porosity of 0.4 and a tortuosity factor of 1.6 are considered in the simulations (Campesi, 2012). Physical properties of the components are taken from the literature (Reid et al., 1977). The convective mass-transfer coefficient is obtained from the Nusselt expression applicable to square-channel structured reactors proposed by Hawthorn (1974). Molecular binary diffusivity is calculated following the semi empirical equation of Fuller et al. (1966). Molecular mixed diffusivity for diluted systems, Knudsen diffusivity and effective diffusivity are calculated according to the guidelines of Froment and Bischoff (1990).

2.2. Numerical solution

The differential equations for the gas phase are integrated using the Gear method (Shampine and Gear, 1979). The differential

equations for the washcoat are discretized by means of second order finite differences, using a grid of equally spaced points. For each axial position, the nonlinear algebraic equations generated by the interior grid points are solved through a Quasi-Newton algorithm.

3. Results and discussion

3.1. Base case

The model results are analysed for a base case of a pilot scale monolithic reactor. Table 3 lists the operating conditions and geometrical characteristics of the reactor. A low inlet ethanol concentration is considered (C_{0Et}=100 mg C/m^3). Gas-phase concentration profiles of ethanol, acetaldehyde and carbon dioxide for the base case are presented in Fig. 2. Ethanol shows a decreasing profile with complete abatement at $z\sim$1.5 cm. The acetaldehyde curve presents a well-defined maximum, and then this intermediate component is completely consumed. Carbon dioxide concentration rises from the reactor inlet, as a result of evolution of the combustion reaction (r_2) as long as acetaldehyde is produced.

Fig. 3a shows the concentration cross-section profiles of ethanol in the gas phase and the washcoat at six different axial positions, for the conditions of Fig. 2. As expected, the ethanol profiles decrease along the x coordinate, while the external and internal concentration gradients are less pronounced towards the reactor outlet. At z=2.5 cm, the ethanol has been completely consumed. Fig. 3b exhibits the behaviour of the acetaldehyde concentration. For axial positions at the left of the maximum (z_{max}=0.34 cm, see Fig. 2), the acetaldehyde profiles increase with x, because of the prevalence of the generation rate (r_1). At z=z_{max}, a flat profile of acetaldehyde is observed in the gas phase and the washcoat, indicating that its generation rate (r_1) is approximately equal to the consumption rate (r_2). For higher axial positions (z=0.75, 1 and 2.5 cm), the acetaldehyde cross-section profiles diminish due to the predominance of Reaction 2 (r_2), i.e., elimination of the intermediary.

The corresponding axial profiles of the effective reaction rates (r_1^{eff} and r_2^{eff}) are included in Fig. 4. The variable r_1^{eff} shows a sharp descending behaviour, which is consistent with the ethanol consumption observed in Figs. 2 and 3a. On the other hand, r_2^{eff} presents a fast increase near the reactor inlet, which is in agreement with the increasing acetaldehyde concentration levels observed in Fig. 2.

Table 3
Geometrical parameters and operating conditions of a pilot scale reactor.

Parameter	Value
Channel length, L	0.05 m
Stack width, W	0.15 m
Channel width=height, b	1115 μm
Cell density	400 cpsi
Total number of channels, NC	13,950
Monolithic material	cordierite ($2MgO\cdot 2Al_2O_3\cdot 5SiO_2$)
Support	Nyacol
Catalytic material	Mn–Cu
Washcoat thickness, δ_w	10 μm
Washcoat density, ρ_w	4030 kg/m^3
Washcoat mass, m_w	124 g
Reaction temperature, T	190–220 °C
Total pressure, P	1 atm
Volumetric feed flow rate, Q_0	37.2 m^3/h
Gas-hourly space velocity, GHSV	1.21×10^6 h^{-1}
Inlet VOC concentration, C_{0Et}	100–300 mg C / m^3
Inlet VOC molar fraction, y_{0Et}	$1.02–3.06\times10^{-4}$

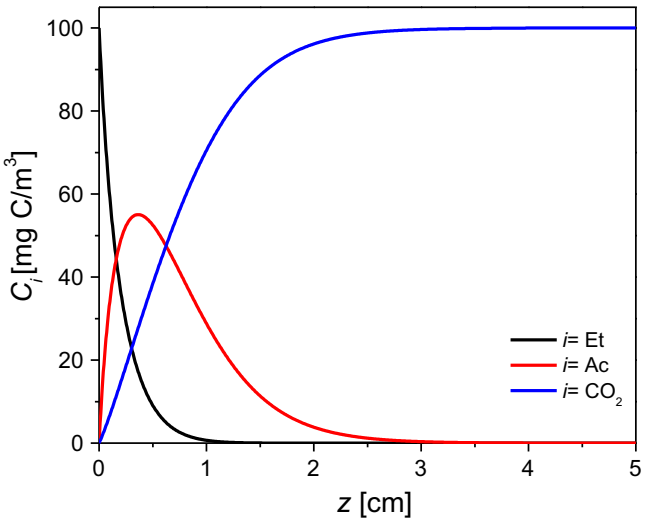

Fig. 2. Axial concentration profiles of ethanol, acetaldehyde and carbon dioxide for the bases conditions: $GHSV$=1.21×10^6 h^{-1}, C_{0Et}=100 mg C/m^3, T=210 °C, m_w=124 g, δ_w=10 μm and NC= 13,950.

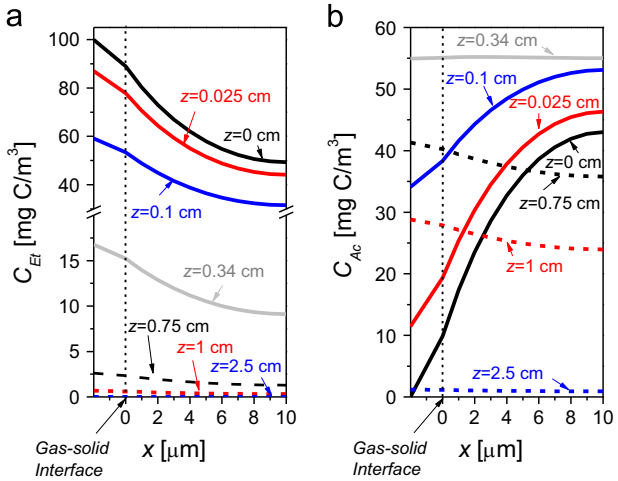

Fig. 3. Transversal concentration profiles of ethanol (a) and acetaldehyde (b) for the conditions of Fig. 2.

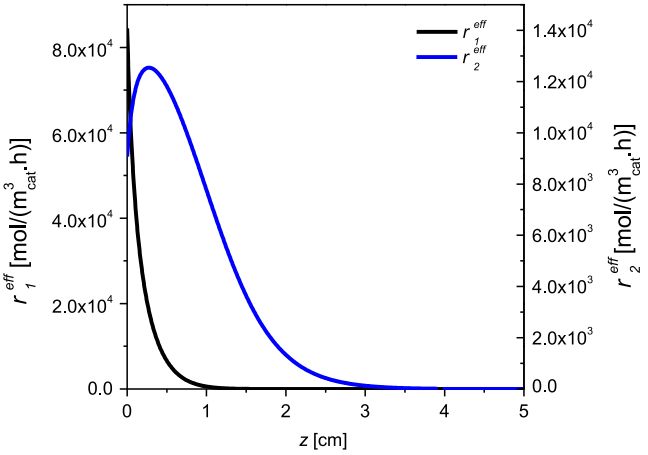

Fig. 4. Evolution of effective reaction rates, r_1^{eff} and r_2^{eff} in the axial reactor coordinate, for the conditions of Fig. 2.

Fig. 5 presents the reaction rate profiles in the washcoat for the reference conditions. Local reaction rates at all the studied axial positions are referred to the corresponding reaction rates at the

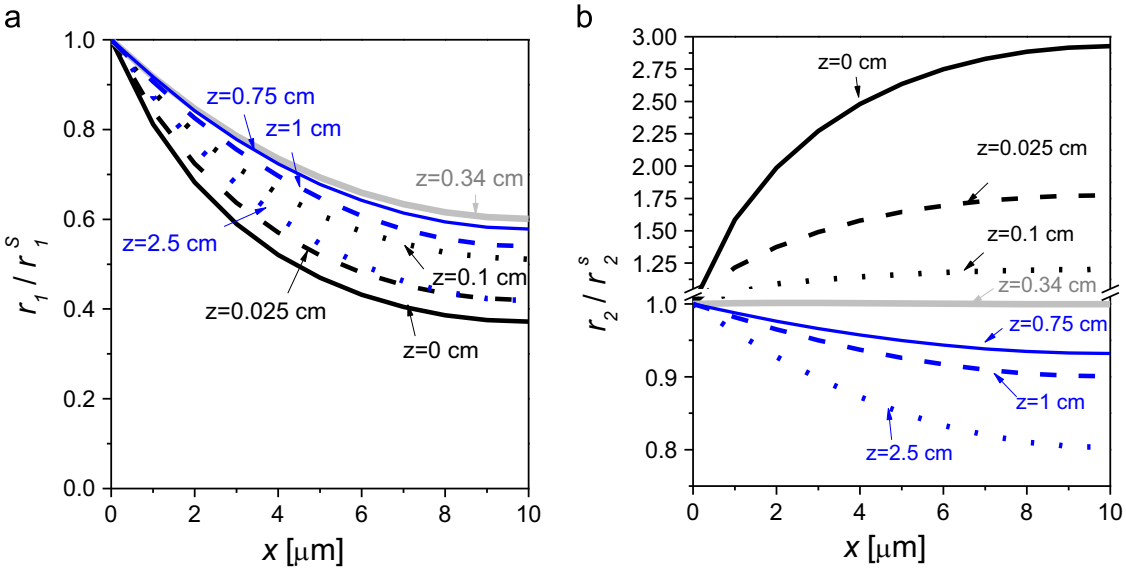

Fig. 5. Evolution of reaction rates r_1/r_1^s (a) and r_2/r_2^s (b) in the washcoat, for the conditions of Fig. 2.

gas-solid interface. As shown in Fig. 5a, the cross-section profiles of r_1/r_1^s are more pronounced at axial positions where the acetaldehyde concentration is low; this phenomenon occurs near the reactor inlet ($z=0$ and 0.025 cm) and beyond $z=2.5$ cm. In fact, despite the very thin washcoat thickness (10 μm), the local values of the reaction rate r_1 at $x=\delta_w$ (interface washcoat/cordierite) become lower than 60% of those calculated at the surface. A similar behaviour is observed for the ratio r_2/r_2^s. When low acetaldehyde concentrations are found (see Fig. 3b) at $z=0$, 0.025 and beyond 2.5 cm, the cross-section profiles of r_2 are more pronounced, either showing a decreasing behaviour (e.g. at $z=2.5$ cm) or an increasing one (e.g. at $z=0$ cm). At these axial positions r_1 and r_2 approximate to first order reactions according to their kinetic expressions (Table 1). Conversely, when C_{Ac} is high enough ($z=0.1$ and 0.34 cm), the behaviour of r_2 approximates to that of a zero order reaction and flat reaction rate transverse profiles are found inside the washcoat.

Increasing r_2/r_2^s profiles mean effectiveness factors for r_2 higher than unity. This tendency is explained from the acetaldehyde concentration profiles observed in Fig. 3b. At positions where acetaldehyde is mainly generated, r_2/r_2^s increases with x, and the local values of the reaction rate r_2 at $x=\delta_w$ become almost 200% higher than those calculated at the surface. In contrast, at axial positions where acetaldehyde is being consumed, r_2 inside the washcoat is lower than that found at the solid surface. The corresponding internal effectiveness factors (for Reactions 1 and 2) at each axial position are reported in Table 4 and they confirm the explanation presented above.

3.2. Influence of ethanol feed concentration

To analyse the influence of C_{0Et}, this operative parameter is modified from its reference value ($C_{0Et}=100$ mg C/m^3). The total catalyst mass, the flow rate and the reaction temperature are kept constant, i.e., $m_w=124$ g, $Q_0=37.2$ m^3/h and $T=205$ °C, respectively.

Fig. 6a and b shows the evolution of effective reaction rates along the axial coordinate (r_1^{eff} and r_2^{eff}), for different ethanol feed concentrations, $C_{0Et}=100$, 200 and 300 mg C/m^3. It can be observed that r_1^{eff} shows a sharp decreasing behaviour, which is in agreement with the total ethanol consumption. Moreover, r_1^{eff} curves shift to the outlet as C_{0Et} increases. On the other hand, r_2^{eff} presents a fast increase near the reactor inlet, because of the condition of higher ethanol feed concentration, and then r_2^{eff} shows a plateau zone at locations where high levels of acetaldehyde are found (r_2 approximates to that of a zero order reaction). This shape of the profile is not observed at conditions where acetaldehyde levels are lower (lower C_{0Et}).

Table 4
Internal effectiveness factor for r_1 and r_2 at the conditions of Fig. 2.

z (cm)	$\eta_{1,int}$	$\eta_{2,int}$
0	0.534	2.436
0.025	0.578	1.567
0.1	0.656	1.143
0.34	0.728	1.001
0.75	0.715	0.955
1.0	0.688	0.934
3.0	0.600	0.868

It is clear that undesirable VOC emissions can be found as the inlet concentration of ethanol increases. However, this conclusion could be different if higher values of C_{0Et} are considered. In these cases thermal effects have to be included in the analysis, since higher values of C_{0Et} would lead to higher temperature increases and, consequently, to faster reaction rates.

Fig. 6c and d, exhibit the evolution of effective, superficial and bulk reaction rates (r_1 and r_2) at axial positions near the reactor inlet, for the same conditions of Fig. 6a and b. It can be observed that at each axial position $r_1^b > r_1^s > r_1^{eff}$, resulting from the ethanol consumption. On the contrary, $r_2^b < r_2^s < r_2^{eff}$, showing an opposite behaviour, i.e., the effectiveness factor for Reaction 2 becomes higher than 1 due to the fact that high acetaldehyde concentrations are found inside the washcoat.

3.3. Influence of operation temperature

Fig. 7 presents ethanol and acetaldehyde axial concentration profiles at four reaction temperatures. As expected, ethanol consumption increases with temperature. The intermediary is slightly consumed at low operation temperatures, indicating that acetaldehyde emissions can be significant even at conditions of total conversion of ethanol (e.g, $T=190$, 200 °C), which is clearly undesirable. For $T=210$ and 220 °C the acetaldehyde profiles present a well-defined maximum, after which the intermediate component is completely consumed.

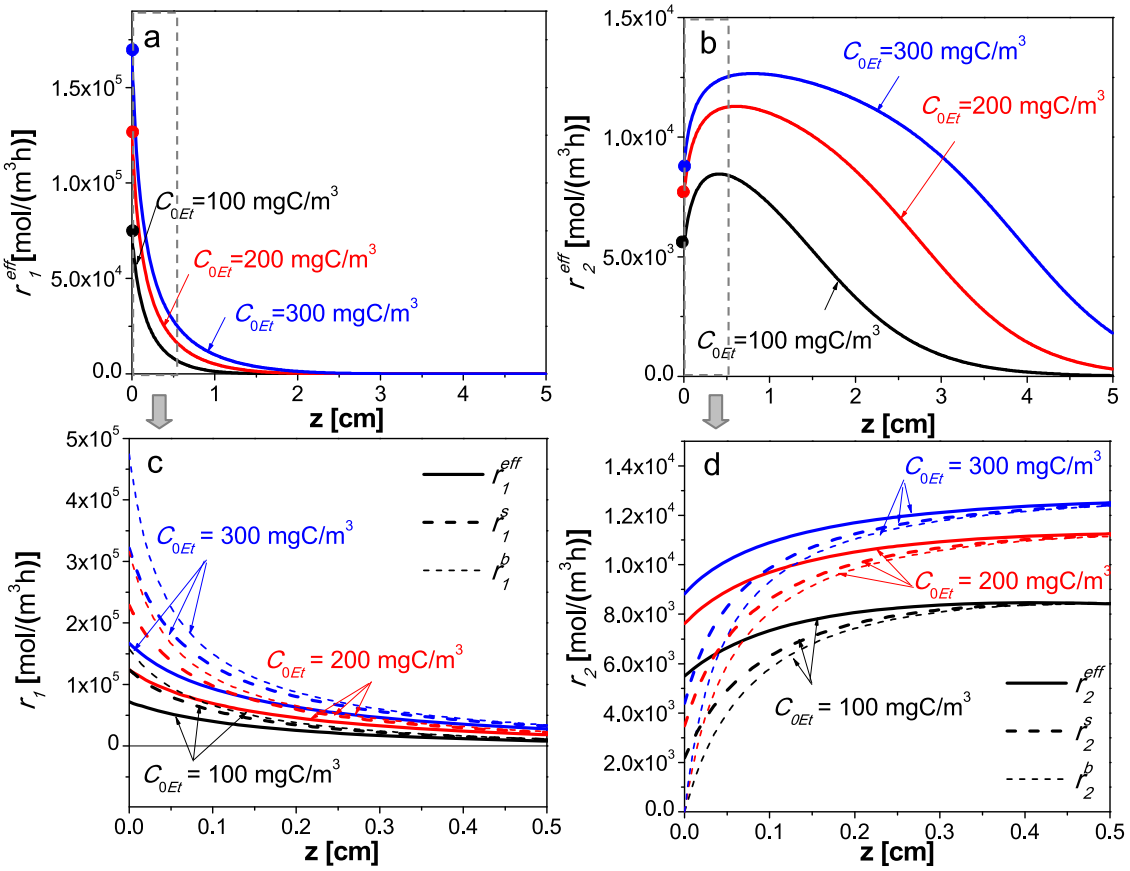

Fig. 6. Evolution of effective, superficial and bulk reaction rates, r_1 and r_2 in the axial reactor coordinate, for different ethanol feed concentration, C_{0Et}=100, 200 and 300 mg C/m^3, $GHSV$=1.21 × 10^5 h^{-1}. T=205 °C, m_w=62.4 g, δ_w=10 μm, and NC= 13,950.

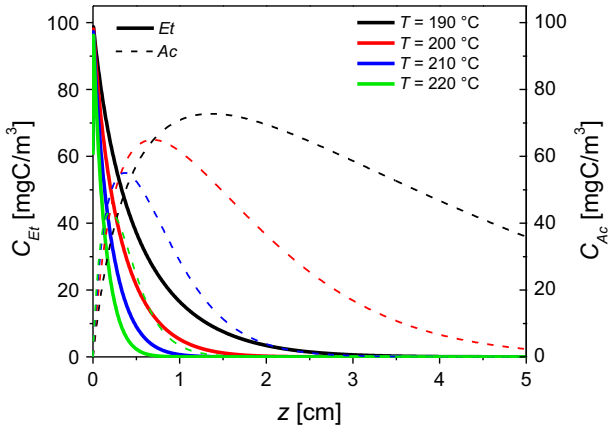

Fig. 7. Axial concentration profiles of ethanol (dashed lines) and acetaldehyde (solid lines), for different operation temperature, T=190, 200, 210 and 220 °C. $GHSV$=1.21 × 10^6 h^{-1}. C_{0Et}=100 mg C/m^3, m_w=124 g, δ_w=10 μm, NC= 13,950.

Fig. 8a and b shows ethanol and acetaldehyde concentration cross-section profiles near the reactor inlet (z=0.005 cm) for the selected temperatures. For the same operating conditions, Fig. 8c and d presents the evolution of reaction rates r_1/r_1^b and r_2/r_2^b, respectively.

The increment in r_1 and r_2 as temperature is increased leads to more pronounced cross-section profiles of ethanol (Fig. 8a) and acetaldehyde (Fig. 8b). The behaviour of the curves r_1/r_1^b is in agreement with the ethanol concentration profiles (Fig. 8a), i.e., the influence of the mass transfer limitations on the rate of consumption of ethanol becomes more relevant and the internal effectiveness factor drops from 0.714 to 0.461 as the temperature increases from 190 to 220 °C. At the same time, the external (gas–solid) concentration gradients grow with temperature. However, the model predicts a more complex dependence of r_2 with the temperature. The acetaldehyde concentration gradients inside the washcoat are more significant as higher temperatures are chosen, i.e., higher r_2^{eff} values can be achieved. Conversely, the internal profiles of r_2 are relatively less pronounced as the temperature increases (see Fig. 8d); therefore, the internal effectiveness factors drop from 2.429 (for T=190 °C) to 2.007 (for T=220 °C). This behaviour finds its explanation in the kinetic expression form. At low reaction temperature, acetaldehyde concentration levels are lower, the inhibition term of r_2 (Kc_{Ac} C_{Ac}) tends to zero and the kinetic expression becomes a first order reaction rate. In contrast, at high temperature the inhibition term of r_2 becomes important and the r_2/r_2^b cross-section profiles are flat, according to a nearly zero order reaction. It is important to notice that these results were obtained for a constant value of the adsorption constant Kc_{Ac}, in accordance with the kinetic model proposed by Campesi et al. (2011).

3.4. Influence of washcoat thickness

Typical average washcoat thicknesses are between 10 and 50 μm (Bhattacharya et al., 2004; Joshi et al., 2010). In order to analyse the influence of washcoat thickness on the reactor performance, this value has been increased from its reference value, (δ_w=10 μm) to 50 μm. The comparison is made maintaining both, the space velocity ($GHSV$=1.21 × 10^6 h^{-1}) and the total transverse area (i.e., constant linear velocity, u=1.23 m/s) constant. The

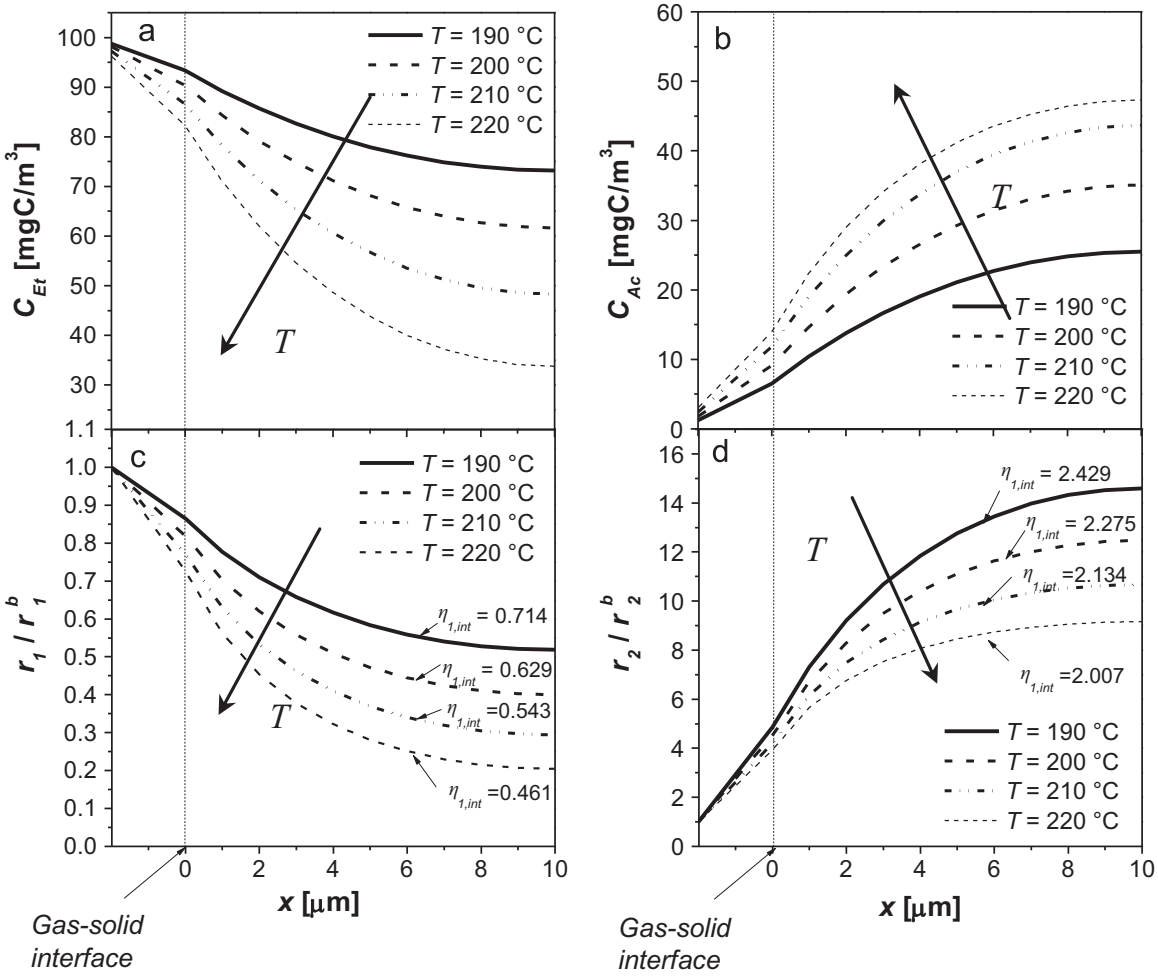

Fig. 8. Transversal concentration profiles of ethanol (a) and acetaldehyde (b) and transversal evolution of reaction rates r_1/r_1^b (c) and r_2/r_2^b (d) at z=0.005 cm for the conditions of Fig. 7.

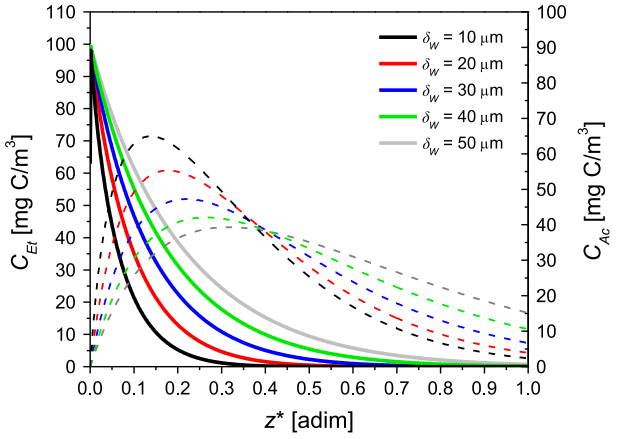

Fig. 9. Axial concentration profiles of ethanol (solid lines) and acetaldehyde (dashed lines), for different washcoat thickness for the same space velocity ($GHSV$=1.21 × 10^6 h^{-1}), i.e., the same total catalyst mass (m_w=248 g) and the total transverse area (i.e., constant linear velocity, u=1.23 m/s), C_{0Et}=100 mg C/m^3, T=200 °C.

reactor length (L) and the number of channels (NC) are adjusted simultaneously to achieve such purpose.

Fig. 9 presents axial ethanol and acetaldehyde concentration profiles for four different arrangements of the catalyst. Table 5 details washcoat thickness (δ_w), number of channels (NC), reactor length (L) and external washcoat surface area per unit washcoat volume (a_v) for each arrangement. C_{0Et}=100 mg C/m^3 and T=200 °C are selected for the simulations. Ethanol conversion decreases as the washcoat thickness increases, due to the fact that higher mass transfer limitations occur. The value of the maximum acetaldehyde concentration is lower as the washcoat thickness increases and its axial location shifts to the outlet. The acetaldehyde slip observed at the reactor outlet increases with the washcoat thickness increment and it is near the emission limit value (20 mg/Nm³) at δ_w=50 μm.

Table 5
Washcoat thickness (δ_w), number of channels (NC), reactor length (L) and external washcoat surface area per unit washcoat volume (a_v) for the five considered arrangements.

δ_w (μm)	NC	L (m)	a_v (m_w^2/m_w^3)
10	13,950	0.100	99,095
20	14,474	0.049	49,087
30	15,028	0.032	32,412
40	15,615	0.023	24,070
50	16,236	0.018	19,061

Fig. 10 shows the axial evolution of internal and external effectiveness factors for r_1 and r_2, at the same conditions of Fig. 9. As it can be seen, internal mass transport resistances become important as the washcoat thickness increases, leading to a significant drop of the internal effectiveness factor for r_1; thus, for δ_w=50 μm the averaged internal effectiveness factor is

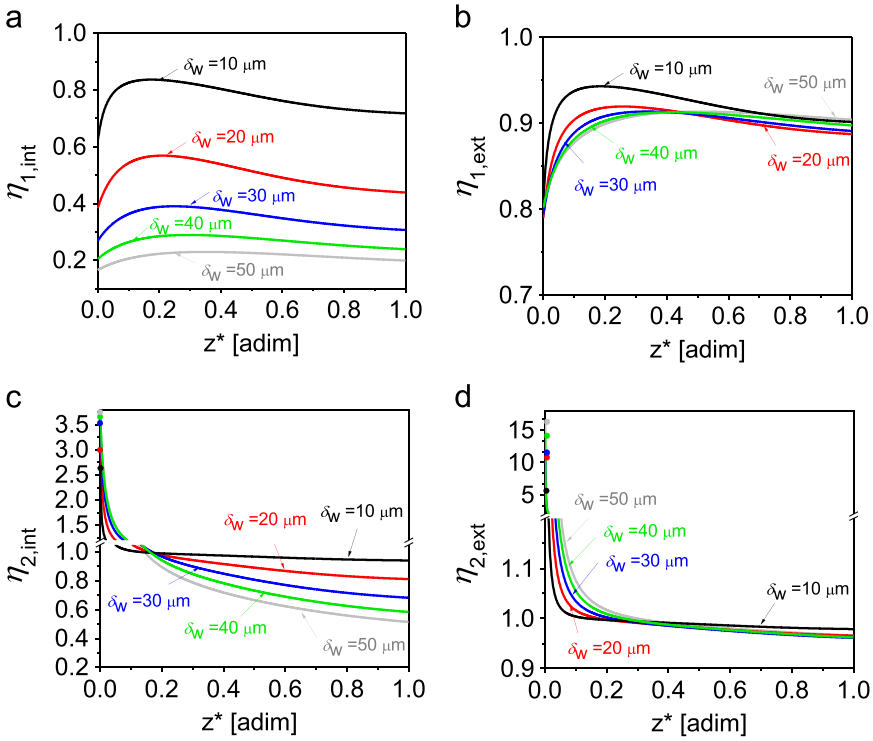

Fig. 10. Axial evolution of internal and external effectiveness factor of r_1 (a and b) and axial evolution of internal and external effectiveness factor of r_2 (c and d), for the same condition of Fig. 9.

$\overline{\eta}_{1,\,int} \sim 0.2$. It is important to notice that, even at this relatively low reaction temperature, mass transfer resistances strongly affect the reaction rate. The external effectiveness factors for r_1 (Fig. 10b) decrease with δ_w. This increase in the external mass transfer resistances as δ_w increases results from the strong decrease of the external washcoat surface area per unit washcoat volume (a_v) (see Table 5), which leads to an increment of the external concentration gradients. On the other hand, internal effectiveness factor of Reaction 2 ($\eta_{2,int}$) increases with the washcoat thickness at axial positions near the reactor inlet, i.e., the zone where acetaldehyde is mainly produced (see Fig. 10c). The increase in the washcoat thickness leads to an increment in the mass transport resistances and more acetaldehyde accumulation in the washcoat. Local reaction rates in x-δ_w are more than 3 times greater than those found in the washcoat surface $x=0$. Conversely, at axial positions where the intermediary is mainly consumed, $\eta_{2,int}$ diminishes as δ_w increases. The decrease in a_v also leads to reaction rates in washcoat surface r_2^s 15 times greater than those found in bulk gas phase r_2^b (see Fig. 10d).

4. Conclusions

The catalyst is active enough for significant diffusional resistances at relatively low operation temperatures. In spite of the fact that a thin washcoat was selected in the simulations (δ_w=10 μm), significant mass transfer limitations were found under certain operating conditions. For thick washcoats and high conversions of VOCs (higher temperatures), the overall process rate is reduced by internal diffusion inside the catalyst. For higher temperatures and/or monoliths with poor interfacial areas, the overall process rate is limited by external mass transfer resistance to the catalyst. Quantifying properly both internal and external mass transfer resistances by means of a heterogeneous model can result in avoiding situations of uncompleted VOC abatement under conditions of high VOC dilution.

Notation

b	channel width=height, mm
C_j	concentration of j component, mol_j/m^3 or mg C/m^3
$C_{s,j}$	concentration of j component in the solid phase, mol_j/m^3 or mg C/m^3
$C^s_{s,j}$	concentration of j component at surface of the solid phase, mol_j/m^3 or mg C/m^3
$D_{e,j}$	effective diffusion coefficient for j component, m^2/s
E_i	activation energy of i reaction, J/mol
$GHSV$	gas-hourly space velocity, h^{-1}
$k_{g,j}$	convective mass-transfer coefficient from gas to solid interface, $m_f^3/(m_i^2\ s)$
$k_{ref,1}$	kinetic constant of Reaction 1, 1/s
$k_{ref,2}$	kinetic constant of Reaction 2, mol/(m^3 s)
Kc_j	adsorption constant of j component, m^3/mol
L	channel length, m
m_w	catalyst mass, g
NC	number of channels
P	total pressure, atm
Pe	Peclet number, adim
Q_0	volumetric feed flow rate, m^3/h
r_i	reaction rate of i reaction, i=1, 2, mol/
r_i^b	reaction rate of i reaction at gas phase, i=1, 2, mol/(m^3_{cat} s)
r_i^{eff}	effective reaction rate of i reaction, i=1, 2, mol/
r_i^s	reaction rate of i reaction at gas-solid inteface, i=1,2, mol/
R	universal gas constant, J/(mol K)
T	reaction temperature, °C
u	average velocity, m/s
V_g	gas volume, m^3
V_w	washcoat volume, m^3
x	transversal coordinate, m
y_j	molar fraction of j component, dimensionless
z	axial coordinate, m

C_2H_5OH	ethanol
C_2H_4O	acetaldehyde
CO_2	carbon dioxide
H_2O	water
O_2	oxygen
C	carbon

Greek letters

δ_w	washcoat thickness, μm
η_i	effectiveness factor of *i* reaction, dimensionless
ρ_w	washcoat density, kg/m^3

Subscripts

Ac	acetaldehyde
Et	ethanol
ext	external
i	*i* reaction
int	internal
j	*j* component
max	maximum
ref	reference
w	washcoat
0	at the axial coordinate $z=0$

Superscripts

b	at bulk gas phase
eff	effective
s	at solid surface

Acknowledgements

Support of this work through Universidad Nacional de San Luis (UNSL) (Grant nos. PROICO-2-0001, 22/Q025), Agencia Nacional de Promoción Científica y Tecnológica (ANPCyT) (Grant nos. PICT 2013-1537, PICT 2010 – 2223) and Consejo Nacional de Investigaciones Científicas y Técnicas (CONICET) (Grant no. PIP: 112-201101-00907) is fully acknowledged.

References

Agüero, F.N., Morales, M.R., Duran, F., Barbero, B.P., Cadús, L.E., 2013. MnCu/Cordierite monolith used for catalytic combustion of Volatile Organic Compounds. Chem. Eng. Tech. 36, 1749–1754.

Air Quality Guidelines: Global Update – World Health Organization (WHO), 2005. Denmark, (⟨http://www.euro.who.int/__data/assets/pdf_file/0005/78638/E90038.pdf⟩).

Avila, P., Montes, M., Miró, E.E., 2005. Monolithic reactors for environmental applications: a review on preparation technologies. Chem. Eng. J. 109, 11–36.

Bhattacharya, M., Harold, M.P., Balakotaiah, V., 2004. Shape normalization for catalytic monoliths. Chem. Eng. Sci. 59, 3737–3766.

Campesi, M.A., Mariani, N.J., Pramparo, M.C., Barbero, B.P., Cadús, L.E., Martínez, O. M., Barreto, G.F., 2011. Combustion of Volatile Organic Compounds on a MnCu catalyst: a kinetic study. Catal. Today 176, 225–228.

Campesi, M.A., 2012. Estudio de sistemas combinados de combustión catalítica de VOCs (Ph.D. thesis). Universidad Nacional de La Plata, Argentina ⟨http://sedici.unlp.edu.ar/bitstream/handle/10915/27082/Documento_completo.pdf?sequence=1⟩.

Chen, J., Yang, H., Wang, N., Ring, Z., Dabros, T., 2008. Mathematical modeling of monolith catalysts and reactors for gas phase reactions. Appl. Catal. A 345, 1–11.

Choudhary, T.V., Banerjee, S., Choudhary, V.R., 2002. Catalysts for combustion of methane and lower alkanes. Appl. Catal. A 234, 1–23.

Ertl, G., Knözinger, H., Schüth, F., Weitkamp, J., 2008. Handbook of Heterogeneous Catalysis, second ed. Wiley-VCH, Weinheim.

Everaert, K., Baeyens, J., 2004. Catalytic combustion of Volatile Organic Compounds. J. Hazard. Mater. B109, 113–119.

Froment, G.F., Bischoff, K.B., 1990. Chemical Reactor Analysis and Design, second ed. Wiley, Toronto, Canada.

Fuller, E.N., Schettler, P.D., Giddings, J.C., 1966. New method for prediction of binary gas-phase diffusion coefficients. Ind. Eng. Chem. 58, 19–27.

Gonzo, E.E., 2008. Hydrogen from methanol-steam reforming: isothermal and adiabatic monolith reactors simulation. Int. J. Hydrog. Energy 33, 3511–3516.

Hayes, R.E., Kolaczkowski, S.T., 1994. Mass and heat transfer effects in catalytic monolith reactors. Chem. Eng. Sci. 49, 3587–3599.

Hayes, R.E., Kolaczkowski, S.T., 1997. Introduction to Catalytic Combustion, first ed. Gordon and Breach Science Publishers, Netherlands.

Hayes, R.E., Liu, B., Moxom, R., Votsmeier, M., 2004. The effect of washcoat geometry on mass transfer in monolith reactors. Chem. Eng. Sci. 59, 3169–3181.

Hawthorn, R.D., 1974. Afterburner catalysis effects of heat and mass transfer between gas and catalyst surface. AIChE. Symp. Ser. 70, 428–438.

Heck, R.M., Gulati, S., Farrauto, R.J., 2001. The application of monoliths for gas phase catalytic reactions. Chem. Eng. J. 82, 149–156.

Heck, R.M., Farrauto, R.J., Gulati, S., 2009. Catalytic Air Pollution Control-Commercial Technology, third ed. Wiley, New York.

Hessel, V., Löwe, H., Müller, A., Kolb, G., 2005. Chemical Micro Process Engineering-Processing and Plants. WILEY-VCH Verlag GmbH & Co. KGaA, Weinheim.

Joshi, S.Y., Harold, M.P., Balakotaiah, V., 2010. Overall mass transfer coefficients and controlling regimes in catalytic monoliths. Chem. Eng. Sci. 65, 1729–1747.

Khan, F.I., Ghoshal, A.K., 2000. Removal of Volatile Organic Compounds from polluted air. J. Loss Prev. Process Ind. 13, 527–545.

Metkar, P., Balakotaiah, V., Harold, M., 2011. Experimental study of mass transfer limitations in Fe- and Cu-zeolite-based NH_3–SCR monolithic catalysts. Chem. Eng. Sci. 66, 5192–5203.

Mitsui, T., Matsui, T., Kikuchi, R., Eguchi, K., 2009. Low-temperature complete oxidation of ethyl acetate over CeO_2-supported precious metal catalysts. Top. Catal. 52, 464–469.

Morales, M.R., Barbero, B.P., Cadús, L.E., 2008. Evaluation and characterization of Mn–Cu mixed oxide catalysts for ethanol total oxidation: Influence of copper content. Fuel 87, 1177–1186.

Reid, R.C., Prausnitz, J.M., Sherwood, T.K., 1977. The Properties of Gases and Liquids, third ed. Mc Graw Hill, New York.

Shampine, L.F., Gear, C.W., 1979. A users view of solving stiff ordinary differential equations. SIAM Rev. 21, 1–17.

The Clean Air Act – Environmental Protection Agency (EPA), 2004. USA, (⟨http://www.epw.senate.gov/envlaws/cleanair.pdf⟩).

Tomasic, V., Jovic, F., 2006. State of the art in the monolithic catalysts/reactors. Appl. Catal. A 311, 112–121.

Wang, X., Daniels, R., Bake, R.W., 2001. Recovery of VOCs from high-volume, low-VOC-concentration air streams. AIChE J. 47, 1094.